Journal of Chromatography A, 1217 (2010) 8062–8071

Contents lists available at ScienceDirect

Journal of Chromatography A

journal homepage: www.elsevier.com/locate/chroma

# Role of the shape of various bacteria in their separation by Microthermal Field-Flow Fractionation

Josef Janča [a,*], Věra Halabalová [b], Jan Růžička [c]

[a] Department of Physics and Materials Engineering, Faculty of Technology, Tomas Bata University in Zlín, Czech Republic
[b] Department of Food Biochemistry and Analysis, Faculty of Technology, Tomas Bata University in Zlín, Czech Republic
[c] Department of Environmental Protection Engineering, Faculty of Technology, Tomas Bata University in Zlín, Czech Republic

ARTICLE INFO

*Article history:*
Available online 30 October 2010

*Keywords:*
Brownian movement
Thermal diffusion
Translational diffusion coefficient
Rotational diffusion coefficient
Non-spherical particles
Microthermal Field-Flow Fractionation
Separation of different shape particles
Biological applications
Gram-positive and Gram-negative bacteria
*Staphylococcus epidermidis*
*Rhodococcus erythropolis*
*Acinetobacter lwoffii*
*Acidovorax* sp.

ABSTRACT

The steady-state movement of the spherical and non-spherical particles, such as prolate or oblate rotational ellipsoids, cylinders, or parallelepipeds, suspended in a liquid and exposed to a unidirectional temperature gradient, is analyzed theoretically. The differences in the ratios of the rotational to translational diffusion coefficients of the non-spherical to spherical particles, the heterogeneity of thermal conductivity of the particle body, and the heterogeneity in surface chemical nature make possible to separate the particles according to differences in shape. Preliminary experimental separations of Gram-positive and Gram-negative, nearly spherical and rod-shaped bacteria performed by Microthermal Field-Flow Fractionation confirmed that the fractionation of the cells according to differences in shape is possible.



## 1. Introduction

Several methods are currently in use for the analytical and preparative separation of living cells and subcellular particles. According to the editors [1], approximately 99 percent of these separations were performed by centrifugation in the eighties of the 20th century. Although the proportion of applications of a centrifuge changed in the meantime, it is still the method of frequent laboratory utilization.

The fractionation of the particulate species by centrifugation can be performed on the basis of differences in particle sizes or densities. Since the product of the size and density determines the rate of sedimentation, a simple measurement of sedimentation velocity in one suspending liquid does not allow an accurate determination of particle size distribution if the density of all particles is not the same. The solution of this problem is to carry out several measurements in suspending liquids of different densities.

On the other hand, the fractionation of the particles in density gradient by so-called "isopycnic focusing" which should provide the fractionation according to density differences may also be complicated. The reason is that, contradictory to the general believe, the famous Archimedes principle suits well to the macroscopic world but not really to the microscopic one [2–4]. Consequently, the fractions obtained by isopycnic focusing and considered as uniform can contain the species of different sizes as well as of different densities.

An additional complication may occur whenever the particles in a mixture fractionated by sedimentation are of different shapes, spherical and non-spherical. In such a case, the fractionation based on the differences in sedimentation velocities is not simple (if not impossible). The complication is due to the fact that the sedimentation of non-spherical particles results in their orientation relative to the direction of sedimentation [5–7]. It has been found by Rong et al. [7] that non-spherical particles (ellipsoids and cylinders of small aspect ratio) which sediment at very low particle Reynolds number turn the long axis vertically but they turn horizontally as particle Reynolds number increases. Particle Reynolds number and, consequently particle orientation, is determined by sedimentation velocity. Reciprocally, sedimentation velocity changes with particle orientation. The aspect ratio of non-spherical axisymetric particles affects the orientation and sedimentation velocity [8]. However, the fibers with different aspect ratio exhibit identical terminal sedimentation velocity if they have the same density and diam-

* Corresponding author. Tel.: +420 57603 5110; fax: +420 57603 2741.
*E-mail address:* jjanca@ft.utb.cz (J. Janča).

0021-9673/$ – see front matter © 2010 Elsevier B.V. All rights reserved.
doi:10.1016/j.chroma.2010.10.082

eter [5]. In concentrated particle suspensions, the orientation and sedimentation velocity of the rods and fibers are hindered by particle hydrodynamic interactions [9–11] and this collective behavior causes that the non-spherical particles align vertically. As a result, the further progress in fractionation of the cells and subcellular particles is possible only by looking for new methods that should be more specific, allowing the separations of the species which differ not only in size or density but exhibit also the differences in shape, flexibility, and in surface nature.

Bigelow et al. [12] have demonstrated long time ago that Field-Flow Fractionation (FFF) can be used not only for the separation of the cells but also for the measurement of surface adhesion forces. Recently, the Microthermal Field-Flow Fractionation (Microthermal FFF) was applied for high-performance, high-speed separation of various living bacteria [13,14]. The dominating focusing mechanism of separation was proven but a fundamental question remains unanswered: On the basis of which parameter the two bacteria exhibiting the similar size, *Staphylococcus epidermidis* and *Rhodococcus erythropolis*, were separated?

Several studies of particle thermophoretic motion have clearly indicated that not only the size and density are the parameters determining the retention in Thermal FFF but that several other particle characteristics may also play an important role in separation mechanism [15]. It has been found empirically that thermal diffusion coefficient depends on the chemical nature of the retained species. It is an important finding but the possibilities of a full exploitation of this phenomenon in particle separations have not yet been systematically investigated.

The goal of this work is a detailed theoretical analysis of the effect of the shape of particulate species on their transport phenomena and an experimental study of the effect of various characteristics of several types of bacteria and of the experimental conditions on the retention in Microthermal FFF. A full understanding of the relations between bacteria characteristics (such as the size, shape, and chemical nature) and separation mechanism determining the retention is important not only from the theoretical point of view but also for an optimal use of the Microthermal FFF in the unconventional analyses and characterizations of the cells and subcellular particles.

## 2. Theory

### 2.1. Retention mechanisms in Microthermal Field-Flow Fractionation

One of two main retention mechanisms, *polarization* or *focusing* [15], can govern the separation in Microthermal FFF. A detailed explanation of the separative and dispersive transport phenomena related to the separation mechanisms were repeatedly explained in numerous papers and can be found in Ref. [15]. In this paper only a brief description is given in the following paragraphs.

*Polarization* mechanism is usually assumed to dominate the fractionation of the macromolecules in solution or of the small particles in suspension whose effective size is less than approximately 1 μm. Nevertheless, it has been found recently that an unmistakable domination of polarization mechanism is rather below particle diameter of approximately 200 nm [15,16]. At a steady state, an exponential concentration distribution of uniform retained macromolecules or particles is formed across the microfluidic separation channel of rectangular cross-section due to the balance between the flux of the particles caused by the action of a thermodynamic force generated by temperature gradient and by the counteracting flux which is due to Brownian motion or Fickian diffusion. The maximum concentration of the particles is at the accumulation wall of the channel, most frequently at the cold wall.

*Focusing* mechanism is generated by the effect of two or more counteracting forces and the resulting force must lead to the converging transport which concentrates each of the fractionated species in a distinct focused zone at a particular focusing position in the direction across the channel. It is generally assumed that this mechanism occurs at relatively high linear velocities of the carrier liquid whenever the effective size of the fractionated species is more than approximately 1 μm, as mentioned above. In this case, so-called lift forces and the counteracting gravitational and external field forces generate the focusing of the particles. The concentration distribution of uniform separated species in a focused zone is similar to but not exactly the Gaussian distribution function [15]. However, detailed experimental studies [15–17] proved that transition range of particle sizes at which polarization mechanism begins to be dominated by focusing mechanism is around particle diameter of 200 nm [16]. Moreover, it has been found that the gravitational force cannot be neglected for the particles as small as 200 nm in diameter and of density $\rho = 1.05\ \mathrm{g/cm^3}$, suspended in water. It means that the condition for focusing mechanism to occur (effective action of lift force and counteracting external field force) is fulfilled at high linear velocities of the carrier liquid even for much smaller particles than generally assumed until now.

Nearly parabolic flow velocity profile is formed in carrier liquid flowing in the longitudinal direction of the microfluidic channel. Consequently, different particles, distributed differently across the channel under the conditions of dominating polarization mechanism or focused at different positions across the channel if focusing mechanism is effective, are transported along the channel with different velocities and are thus separated.

The action of a particular retention mechanism in Microthermal FFF is determined by the imposed experimental conditions such as the temperature difference across the channel and the linear velocity of the carrier liquid but also by the characteristics of the retained particulate species, such as the mass, size, density, surface chemical nature or other surface properties.

Two above mentioned primary retention mechanisms can be accompanied by secondary mechanisms and interactions. Consequently, the final driving force, $F(x)$, acting on a single retained particle suspended in a carrier liquid, can be position-dependent and composed of several contributing forces resulting from the secondary mechanisms [15,17]. The driving force can be formally described by Eq. (1):

$$\pm F(x) = \mp F_{TD} - F_G \mp F_{FD} \mp F_{AD} \mp F_{AI}(x) \pm F_{RI}(x) \pm F_{LF}(x) \quad (1)$$

where $F_{TD}$ is the thermodynamic force generated by temperature gradient, $F_G$ is the force which results from the action of the gravitation and buoyancy, $F_{FD}$ is the force caused by friction drag of the particle against the accumulation wall, $F_{AD}$ is the force generated by the adsorption of the separated species at the accumulation wall, $F_{AI}(x)$ is particle–particle attractive interaction force, $F_{RI}(x)$ is particle–particle repulsive interaction force, and $F_{LF}(x)$ is lift force. The positive or negative sign is assigned to each of the contributing forces in Eq. (1) with regard to the position $x = 0$ at the cold wall of the channel and to the positive direction of the $x$-axis from the cold to the hot wall across the channel. The forces $F_{AI}(x)$ and $F_{RI}(x)$ can vary with the $x$-coordinate because they can depend on the concentration of the particles which itself varies with the $x$-coordinate. Lift force $F_{LF}(x)$ is also position-dependent. Moreover, its relative magnitude determines the primary retention mechanism: *polarization* mechanism is effective if $\left|F_{TD} \pm F_G\right| \gg F_{LF}(x)$ and *focusing* mechanism is effective if $\left|F_{TD} \pm F_G\right| \approx F_{LF}(x)$ and, consequently, $F_{AD} = F_{FD} = 0$. In the latter case, the forces $F_{AI}(x)$ and $F_{RI}(x)$ do not contribute to the retention but to the broadening of the focused zone [15]. On the other hand, whenever polarization mechanism is dominant, the force $F_{LF}(x)$ should be negligible, as mentioned above.

Whenever focusing mechanism is dominant, Eq. (1) reduces to:

$$\pm F(x) = \mp F_{TD} - F_G \pm F_{LF}(x) \quad (2)$$

The consequences of the forces $F_{AI}(x)$ and $F_{RI}(x)$ are different in this case. Although both $F_{AI}(x)$ and $F_{RI}(x)$ contribute to the change of the width of the focused zone in the direction of the focusing force, as mentioned above, the force $F_{AI}(x)$ leads to the sharpening of the zone whereas the force $F_{RI}(x)$ broadens the zone. However, if $F_{AI}(x)$ is not negligible, the occurrence of particle aggregation can influence the retention.

Direct measurement of the above mentioned forces by Microthermal FFF is usually not possible. However, the total driving force can be determined from the retention data (namely from retention ratio $R$ defined below) and the contributing forces can be evaluated by a suitable variation of the experimental conditions by which some particular contributing force or forces can be minimized in order to make dominant only one force, if possible, or several different combinations of forces, and thus to elucidate (by a deconvolution procedure) each particular force.

Retention ratio $R$ is defined as the ratio of average linear velocity of the retained species, $v_r$, to average linear velocity of the carrier liquid, $\langle v(x)\rangle$, or more conveniently as the ratio of the retention volume of the unretained species, $V_0$, to the retention volume of the retained species, $V_r$. All mentioned parameters are easily obtained from the experiments.

$$R = \frac{v_r}{\langle v(x)\rangle} = \frac{V_0}{V_r} \quad (3)$$

The combination of Eqs. 2.64, 3.9, and 3.20 from Ref. [15] results, with regard to the force $F_{TD}$, in:

$$F_{TD} = \frac{D_T}{D}\left(\frac{dT}{dx}\right) \cong \frac{D_T}{D}\frac{\Delta T}{w} \quad (4)$$

where $D$ is diffusion coefficient of the retained species, $D_T$ is thermal diffusion coefficient, $dT/dx$ is temperature gradient across the Microthermal FFF channel, $\Delta T$ is temperature difference across the channel, and $w$ is the channel thickness or, in other words, the distance between the accumulation and depletion walls of the channel. Eq. (4) clearly shows how the thermodynamic force $F_{TD}$ in Eqs. (1) and (2) is related to the coefficients $D$ and $D_T$. It follows also from the approximate relationships 2.62 2.64, and 2.65, given in Ref. [15], and from Eqs. (3) and (4) that:

$$R = \frac{6k_B T D}{D_T \Delta T} \quad (5)$$

where $k_B$ is Boltzmann constant and $T$ is the temperature (usually at the accumulation wall of the channel). As a result, Eqs. (1)–(5) demonstrate the impact of the coefficients $D$ and $D_T$ on the retention ratio $R$ determined from Microthermal FFF data for which it holds at an experimental steady state that $F(x) = 0$ in Eqs. (1) and (2).

Previous qualitative observation that *S. epidermidis* and *R. erythropolis* bacteria [13] can effectively be separated by Microthermal FFF stimulated an interest to investigate in detail the physical and physico-chemical backgrounds of this first successful separation of the bacteria generated by thermophoresis. An obvious difference between the two bacteria is in their shape. While *S. epidermidis* are nearly spherical cells, *R. erythropolis* are rods. Consequently, with regard to the above relationships, the theoretical analysis of diffusive, Brownian, and thermophoretic motion of the spherical and non-spherical particles should be the starting point of the study.

### 2.2. Brownian movement of hard spherical and non-spherical particles

The translational diffusion coefficient $D$ of a hard sphere is given by the well-known Einstein–Stokes [18–20] relationship:

$$D = \frac{k_B T}{6\pi\mu r} \quad (6)$$

where $T$ is the temperature, $\mu$ is the dynamic viscosity of the suspending liquid, and $r$ is the radius of the rigid spherical particle. The rotational diffusion coefficient $D_\omega$ of a spherical particle is given by [18]:

$$D_\omega = \frac{k_B T}{8\pi\mu r^3} \quad (7)$$

The translational diffusion coefficient of a non-spherical particle, freely rotating in a three-dimensional (3-D) space, is smaller than that of a sphere of the same volume because of the increased surface area in contact with the liquid and thus the increased friction [20]. The hydrodynamic behavior of a non-spherical particle transported by the flow is complicated because the particle can be oriented as mentioned in the Introduction. However, at a very low particle Reynolds number, shear stress producing the orientation can be compensated by Brownian motion.

The translational diffusion coefficient of the rotational ellipsoid, which can be considered as a model of a non-spherical particle, can be compared with the translational diffusion coefficient of an equivalent sphere having the same volume as the rotational ellipsoid. The ratio of the translational diffusion coefficient, $D_e$, of a rotational ellipsoid to the diffusion coefficient, $D$, of a spherical particle of the same volume was derived by Perrin [21]:

$$\frac{D_e}{D} = \frac{\rho_e^{2/3}}{\sqrt{1-\rho_e^2}} \ln\left(\frac{1+\sqrt{1-\rho_e^2}}{\rho_e}\right)$$

for a prolate ellipsoid for which $\rho_e < 1$ (8)

and:

$$\frac{D_e}{D} = \frac{\rho_e^{2/3}}{\sqrt{\rho_e^2-1}} \arctan\sqrt{\rho_e^2-1}$$

for an oblate ellipsoid for which $\rho_e > 1$ (9)

where $\rho_e = b/a$ is the axial ratio of a rotational ellipsoid ($a$ = length of the axis of the rotation, $b$ = maximal equatorial diameter).

The behavior of the rods for which $\rho_e \gg 1$, the ratio $D_e/D$ can be approximated by [22]:

$$\frac{D_e}{D} = \frac{l_r}{\ln(l_r)} \quad (10)$$

where $l_r$ is the length of the rod. The dependences of the ratios of the translational diffusion coefficients, $D_e/D$, of the non-spherical to spherical particles on the axial ratio, $\rho_e$, for oblate ellipsoids or on its inverse value, $1/\rho_e$, for prolate ellipsoids, are demonstrated in Fig. 1. There is only a minor difference between these two dependences. In comparison with the spherical particles, the decrease of the diffusion coefficient of the rotational ellipsoid is roughly by 20% for $\rho_e = 5$ or $1/\rho_e = 5$. However, even this difference can be sufficient for the separation of the spherical from non-spherical particles by Microthermal FFF, under the condition that no other effects occur.

The ratio of the rotational diffusion coefficient, $D_{\omega,e}$, of a rotational ellipsoid to the rotational diffusion coefficient, $D_{\omega,e}$, of a spherical particle of the same volume was derived by Gans [23] and Perrin [24], however Perrin's solution is preferred here for the reasons of homogeneity.

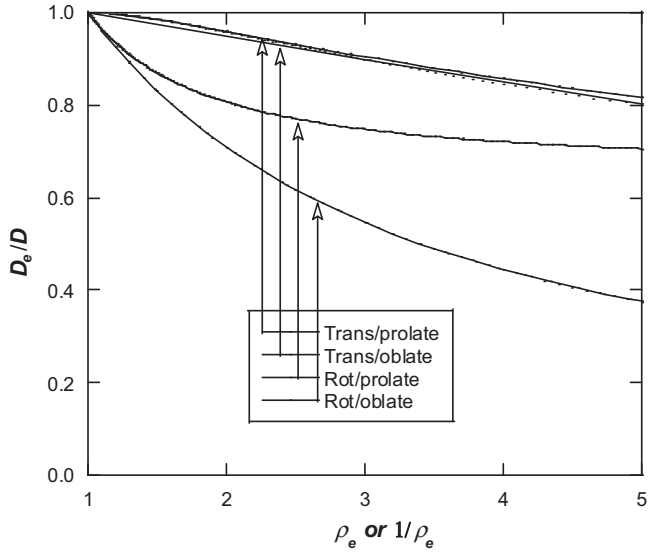


**Fig. 1.** Dependence of the ratios of the translational and rotational diffusion coefficients of the spherical particles to the diffusion coefficients of the rotational ellipsoids, $D_e/D$ (for prolate and oblate ellipsoids) on the axial ratio $\rho_e$ of a rotational ellipsoid or on its reciprocal value $1/\rho_e$, calculated from Eqs. (9)–(12).

This ratio is for a prolate ellipsoid:

$$\frac{D_{\omega,e}}{D_\omega} = \frac{2(\rho_e^2 - 1)/3}{[1 - (\rho_e^2/\sqrt{1-\rho_e^2})\ln((1+\sqrt{1-\rho_e^2})/\rho_e)]} \quad \text{for which } \rho_e < 1 \tag{11}$$

and for an oblate ellipsoid:

$$\frac{D_{\omega,e}}{D_\omega} = \frac{2(\rho_e^2 - 1)/3}{[(\rho_e^2/\sqrt{\rho_e^2-1})\arctan(\sqrt{\rho_e^2-1}) - 1]} \quad \text{for which } \rho_e > 1 \tag{12}$$

The dependences of the ratios of the rotational diffusion coefficients, $D_{\omega,e}/D$, of the non-spherical to spherical particles on the axial ratio, $\rho_e$, for oblate ellipsoids or on its inverse value, $1/\rho_e$, for prolate ellipsoids, are demonstrated in Fig. 1. There are important differences between these two dependences. The decrease of the ratio $D_{\omega,e}/D$ with $\rho_e = 5$ or $1/\rho_e = 5$ for oblate or prolate ellipsoids, respectively, is much more important for oblate ellipsoids. This is easily understandable because the surface to volume ratio of the particle is higher for oblate ellipsoids. In comparison with the spherical particles, the decrease of the rotational diffusion coefficients of the ellipsoids is roughly by 63% for $\rho_e = 5$ of an oblate ellipsoid and by 30% for $1/\rho_e = 5$ of a prolate ellipsoid. The rotational diffusion coefficients should compete with a casual orientation of the particles in temperature gradient, discussed in the following paragraph, and thus influence the retention ratio.

It can be concluded from the above analysis and the results shown in Fig. 1, and with regard to Eq. (4), that the differences between diffusion coefficients of the spherical and non-spherical particles have a direct impact on the thermodynamic force $F_{TD}$ and, consequently, on the retention ratio $R$ as defined by Eq. (3). Moreover, the differences in rotational diffusion coefficients of the spherical and non-spherical particles should allow the separation of the spherical from non-spherical particles by Microthermal FFF even more efficiently in comparison with the effect of differences in translational diffusion coefficients on such a separation.

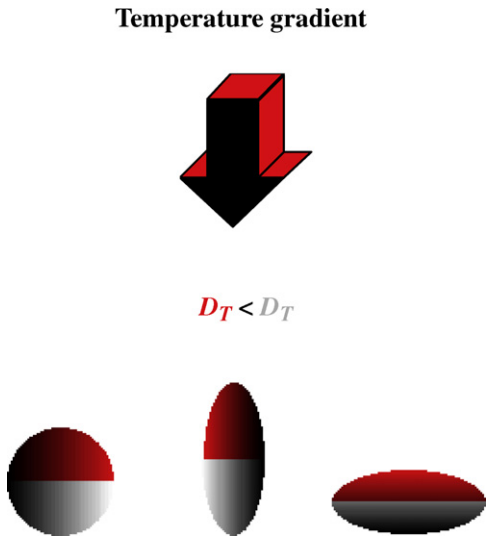


**Fig. 2.** Schematic representation of the orientation of the spherical and non-spherical particles exposed to temperature gradient and exhibiting heterogeneous nature of their surfaces and thus the differences in thermal diffusion coefficients of different parts of particle surfaces. A part of a particle (spherical or non-spherical) which shows higher thermal diffusion coefficient (grey part in comparison with the red part) moves faster by thermophoresis when exposed to temperature gradient and it results in the rotation of the particle until a stable position (shown here for both spherical and non-spherical particles) is reached. (For interpretation of the references to color in this figure legend, the reader is referred to the web version of the article.)

### 2.3. Orientation of the particles exposed to temperature gradient

The thermophoresis should produce similar effect like the sedimentation [7] caused by the gravitational or centrifugal forces. It means that parallel or perpendicular orientation (with regard to the driving force which selectively displaces non-spherical particles in a suspending liquid) should occur independently of the physical character of the driving force. Temperature gradient which generates the thermophoresis of the particles should entrain their orientation as a function of the rate of thermophoretic motion.

The rate of thermophoretic motion is quantitatively described by thermophoretic mobility of a particle, $\mu_T$, which is proportional to the gradient of the temperature, $dT/dx$, to which the particle is exposed:

$$\mu_T = -D_T \frac{dT}{dx} \tag{13}$$

It is a well known empirical fact that $D_T$ is practically independent of particle size but it strongly depends on the chemical nature of the thermophoretically migrating species. As concerns the particles, it is the chemical character of the surface shell and not of the inner core which determines the thermophoretic mobility. The other factors like ionic force of the carrier liquid, pH, etc., also influence the amplitude of $D_T$. Recent paper [25] reviews and systematically classifies all published data on these phenomena, and brings some new experimental findings as well as their explanations.

As a result, the dependence of $D_T$ on the chemical character of particle surface suggests that the particles possessing the topographical heterogeneity in chemical character of their surface can exhibit an orientation when exposed to temperature gradient even in a steady state established by a balance between the flux caused by the thermophoresis and the opposed entropy driven dispersive flux (diffusion or Brownian motion). This hypothesis is schematically demonstrated in Fig. 2 for spherical as well as for non-spherical particles.

Temperature gradient can generate the orientation of a particle also if the particle is not homogeneous with regard to thermal conductivity of its body. The movement of a non-spherical particle (for which one of the dimensions prevails) or of a spherical particle exhibiting spatial heterogeneity in thermal conductivity exposed to a unidirectional temperature gradient could be different in comparison with the particles homogeneous with regard to thermal conductivity.

As described in the previous section, each particle in a stationary isothermal liquid, thus not exposed to temperature and flow velocity gradients, is subject to a free translational and rotational Brownian movement. The mean angular velocity $\omega_{x,y,z}$ of the rotating particle is constant, provided that sufficiently long period of time is considered. Such a uniform rotation is equivalent to presence of two field forces, centrifugal and Coriolis, the later is negligible compared to the first one. The condition of thermal equilibrium of the rotating particle is [26]:

$$\mu_0(P,T) - \frac{1}{2}\sum_a M_a \omega_{x,y,z}^2 r_a^2 = const. \tag{14}$$

where $\mu_0$ is the chemical potential of the particle at rest and $r_a$ is the distance of the $a$-th part of the whole rotating body of the mass $M_a$ from the centre of rotation. The second term in Eq. (14) represents the kinetic energy of the rotational movement. The total energy $E$ of the closed system of a suspension of the particulate components $k$ (undergoing the Brownian movement) is constant in thermal equilibrium [27]:

$$E = U + \frac{1}{2}\sum_k M_k u_k^2 + \frac{1}{2}\sum_k \sum_a M_a \omega_{x,y,z}^2 r_a^2 = const. \tag{15}$$

where $U$ is the internal energy not associated with the Brownian movement and $u$ is the linear velocity of the Brownian movement. The second term in Eq. (15) then corresponds to the energy of the translational Brownian movement and the third one to the rotational Brownian movement.

Let a non-spherical particle or a spherical particle exhibiting spatial heterogeneity in thermal conductivity is suspended in a stationary liquid and exposed to a unidirectional temperature gradient $dT/dx$. The temperature in the steady state of such a non-equilibrium system is not uniform but well defined locally. The entropy production $\sigma$ due to the heat conduction across the particle can be written as [27]:

$$\sigma = \sum_{i=1}^{3} J_{qi} \frac{\partial}{\partial x}\left(\frac{1}{T}\right) = \sum_{x,y,z}\left(\sum -\kappa_{k;x,y,z}\nabla\frac{1}{T}\right)\nabla\frac{1}{T}$$

$$\equiv \sum_k \frac{ds_{k,t}}{dt} \geq 0 \tag{16}$$

$$\sigma = \sum_k J_k \frac{\partial}{\partial x}\left(\frac{1}{T(x)}\right) \equiv \sum_k \frac{ds_{k,t}}{dt} \geq 0$$

where $J_{q;x,y,z}$ is the local flow of heat, $\kappa_{k;x,y,z}$ is temperature dependent local value of the thermal conductivity of the $k$-th part of the particle, $s_{k,t}$ is local entropy density (entropy per unit volume) of a $k$-th part of the particle at a time $t$. The relationship between the flow of heat and thermal conductivity is determined by Fourier's law:

$$J_{q;x,y,z} = -\kappa\nabla T \tag{17}$$

where $\kappa$ is the heat conductivity. The components $J_{q;y}$ and $J_{q;z}$ are non-zero only during the rotational Brownian movement of the particle and thus should not be considered for a steady-state position of the particle at rest. Eq. (16) is an extension of the Second Law of thermodynamics. It postulates that the entropy production due to the irreversible processes must be positive in each part of the system (of the particle body in this case) in the steady state as well as during the transition of the system to a steady state.

Each particle undergoes a 3-D rotational Brownian movement. However, only its rotation in all planes parallel to $dT/dx$ generates the fluctuation of the heat flow across the particle, under the condition that either $\kappa$ across the particle or $dT/dx$ or both are not constant. The fluctuation of the heat flow during the rotation occurs also if the particle exhibits an asymmetry at least with regard to one of three orthogonal axes like, for example, an U-shaped particle. Trivial numerical calculus using Fourier's law can prove this fact. On the other hand, if the axis of the rotation is parallel to $dT/dx$, the heat flow across the particle is constant in the steady state of the whole system.

By supposing that $\kappa$ is not constant within the temperature range of the extreme ends of the particle, it is obvious that, for example, if a parallelepiped of three side dimensions $a = b < c$ is oriented by the side $c$ parallel to $dT/dx = const.$, the flow of heat across the whole particle body is minimum compared to the orientation of the side $a$ or $b$ parallel to $dT/dx$ at which the flow of heat reaches its maximum. The same observation holds for any non-spherical particle such as the rotational ellipsoids, cylinders, etc.

If the particle rotates from its extreme position, the longest $c$ side parallel to $dT/dx$, to any other inclined position with respect to $dT/dx$ axis, the heat flow $J_{q,x}$ across the particle increases and the condition of the positive entropy production due to the rotation, imposed by Eq. (16), is respected. On the other hand, the particle oriented by its side $c$ perpendicular to $dT/dx$ cannot rotate in the planes parallel to $dT/dx$ because such a rotation should result in a decrease in the heat flow $J_{q,x}$ and, consequently, in a prohibited negative value of entropy production. As a result, the rotational Brownian movement generates the entropy driven perpendicular orientation of the longest axis of a non-spherical particle with respect to the temperature gradient. Once the particle achieves this oriented position, its free Brownian rotational movement is possible only around its axis parallel to $dT/dx$. The Second Law of thermodynamics of irreversible processes postulates the identical restriction of the free Brownian rotational movement for the spherical particles. Nevertheless, this restriction should not lead to a change in thermal diffusion and to a change in unidirectional molecular diffusivity of spherical particles like in the case of non-spherical particles.

It follows from the above theoretical analysis that not only the differences in translational diffusion coefficients and in thermal diffusion coefficients of the particulate species can be exploited for their effective separations. The differences in rotational behavior of the particles exposed to temperature gradient make possible to separate the particles according to differences in shape, in heterogeneity of thermal conductivity of particle body, and/or in surface chemical nature heterogeneity.

### 2.4. Effect of hydrodynamic flow

It is a well known fact that the particles transported by a hydrodynamic flow are exposed to shear stress caused by the flow velocity profile established in carrier liquid. If the particle is spherical, it will be forced to rotate due to its exposal to flow velocity gradient. This rotation can be in competition with the orientation of the particle caused by its surface chemical heterogeneity or thermal conductivity. Moreover, the hydrodynamic interactions at higher concentrations of the particles in suspension can lead to collective behavior which still remains rather unclear.

If the particle is not spherical and not oriented at a steady state due to the action of temperature gradient it can be forced

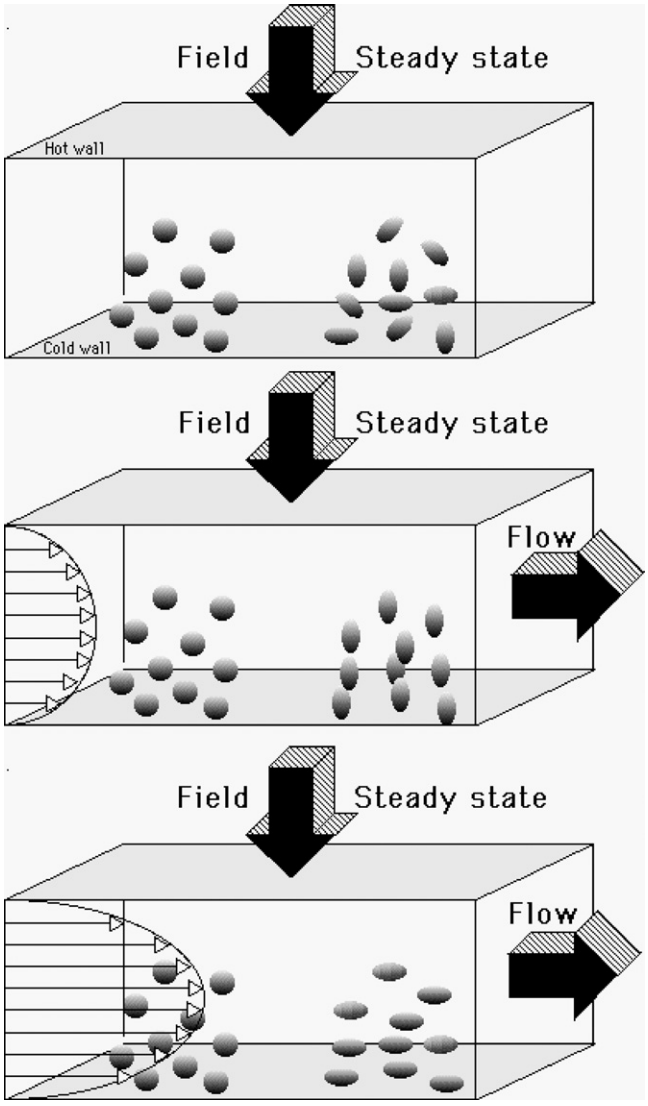


**Fig. 3.** Schematic representation of various situations which can occur when the spherical and non-spherical particles are exposed to temperature gradient under steady-state conditions without the hydrodynamic flow of the carrier liquid and when the particles are transported longitudinally, also under steady-state conditions, by the low (central scheme) or high (bottom scheme) flow-rate of the carrier liquid.

to be oriented in flow velocity gradient. The possible situations are schematically shown in Fig. 3. Temperature gradient combined with the opposite diffusive flux generates, in the absence of the hydrodynamic flow, a steady state with a stable concentration distribution of the spherical or non-spherical particles across the channel. When the longitudinal flow of carrier liquid is applied, the particles undergo the action of lift forces which displace the particles to a new dynamic steady-state position, where the particles are focused. During this displacement, the particles can be oriented vertically or horizontally according to the ratio of the rate of vertical focusing transport to the velocity of longitudinal transport which determines flow velocity gradient in carrier liquid.

The preliminary experimental results described in the following sections indicate that the above theoretical analysis shows very realistic ways to particle separations. Thus the particulate species like the cells and subcellular particles can be separated not only on the basis of size and density differences but also according to shape diversity.

## 3. Experimental

A versatile Microthermal FFF setup was described in detail previously [14]. Versatility of the channel allows an easy change of its thickness and thus its easy adaptability and optimization of the experimental conditions for the separation of the particular species. The dimensions of the Microthermal FFF channel used in this work were 76 mm × 3.2 mm × 0.1 mm. A variable wavelength detector (Watrex UVD 250, Czech Republic) equipped with 1 μL measuring cell was used to record the fractograms at the wavelength of 260 nm.

Deionized water and aqueous NaCl solutions of different concentrations from 3 to 150 mM/L were used as carrier liquids. The optimized injection-stop-flow-time procedure was applied in Microthermal FFF experiments. The injection at the low flow-rate of 0.005 mL/min was carried out during 25 s to introduce the sample into the channel with a minimum zone broadening. Thereafter, the flow rate was stopped for 5 min to allow the establishment of a steady-state concentration distribution of the sample across the channel thickness. Finally, the flow-rate was restarted at different higher values. The temperature of the cold wall, $T_c = 21\,^{\circ}C$, was kept constant in all experiments. Relatively low temperature difference $\Delta T = 33\,^{\circ}C$ across the separation channel was chosen to prevent bacteria denaturation.

Four different bacterial species were used in this study. *S. epidermidis* are Gram-positive spherical cocci that are common members of the normal skin and mucous membranes microflorae. *R. erythropolis* are also Gram-positive but rod-shaped bacilli occurring in soils, waters, and activated sludges. *Acinetobacter lwoffii* is a Gram-negative, non-motile species which exhibits preponderantly a coccobacillary morphology when grown on nonselective agar. It is widely occurring in nature. *Acidovorax* sp. is a genus of Gram-negative aerobic bacteria commonly living in water and soil environments. This species is usually rod-shaped. The above mentioned species were selected in order to represent Gram-positive and Gram-negative cocci and rods.

The particles of the spherical polystyrene latex (PSL) of the diameter of 1 μm were used for the direct experimental comparison of their behavior with the behavior of the bacteria, investigated under the identical experimental conditions of Microthermal FFF. The experimental data for larger size (5.3 μm in diameter) PSL and for spherical silica particles (5.0 μm in diameter) were also used in this study in order to demonstrate the effect of the size and density on the retention. Unfortunately, a direct comparison of their experimental retentions with the data obtained for 1 μm PSL particles and bacteria cells is not possible because the experimental conditions of Microthermal FFF had to be chosen different in this case. Temperature difference applied in the experiments with the bacteria and 1 μm PSL particles would be too high for larger size and higher density particles and thus temperature difference applied in this case was $\Delta T = 0\,^{\circ}C$.

## 4. Results and discussion

### 4.1. Retention of Gram-positive bacteria

The results of Microthermal FFF obtained with PSL particles and with *S. epidermidis* and *R. erythropolis* cells are presented in Fig. 4 as a dependence of the retention ratio $R$ on the average linear velocity of the carrier liquid $\langle v(x)\rangle$. Although the results for 5.3 μm PSL and for 5.0 μm spherical silica particles were obtained under different experimental conditions, they are also given in Fig. 4 in order to show the effect of the density of the particles on the retention. It can be seen in Fig. 4 that all particulate species exhibit more or less strong dependences of $R = f(\langle v(x)\rangle)$ regardless their size, density,

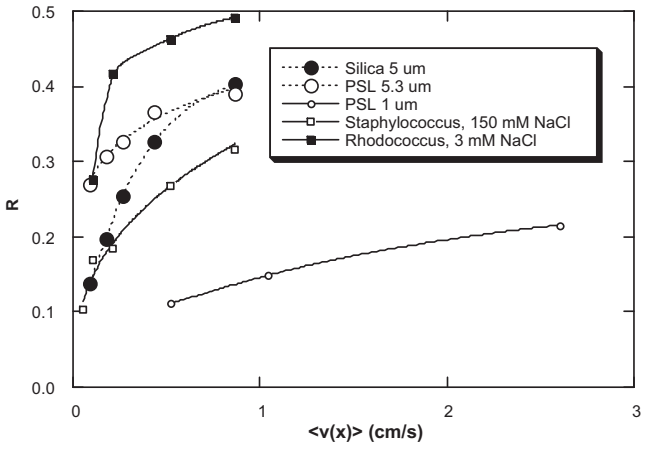


**Fig. 4.** Dependences of the retention ratio $R$ on the average linear velocity of the carrier liquid $\langle v(x)\rangle$ for different polystyrene latex and silica particles and for *Staphylococcus epidermidis* and *Rhodococcus erythropolis* bacteria. Experimental conditions: temperature of the cold wall $T_c$ = 21 °C, $\Delta T$ = 33 °C, linear velocity of the carrier liquid during the elution $\langle v(x)\rangle$ = 0.208 cm/s.

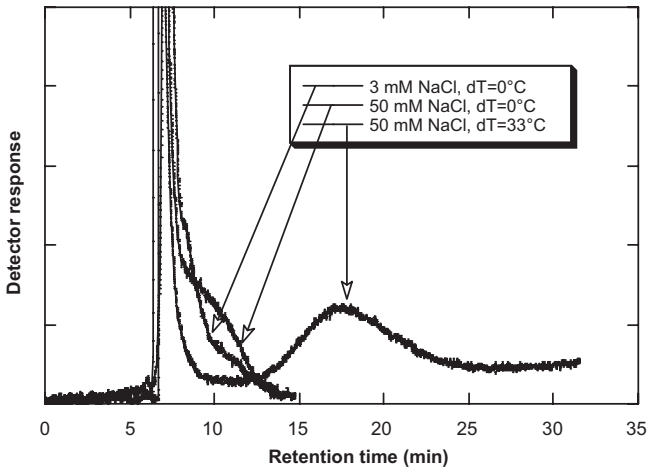


**Fig. 5.** Fractograms of *Staphylococcus epidermidis* cells obtained under different experimental conditions of Microthermal Field-Flow Fractionation. Experimental conditions: temperature of the cold wall $T_c$ = 21 °C, linear velocity of the carrier liquid during the elution $\langle v(x)\rangle$ = 0.208 cm/s, temperature difference, $\Delta T = dT$ is given for each particular experiment.

and nature (or chemical character). This is a proof of the dominant focusing mechanism which was explicitly confirmed by previous detailed studies [16,25] in which the same or similar PSL and silica particles were used. The first such observation of the impact of lift forces on the retention ratio and, consequently, of the occurrence of focusing behavior in FFF of micrometer-sized particles was published by Caldwell et al. [28].

The comparison of the dependence $R = f(\langle v(x)\rangle)$ in Fig. 4 for PSL 5.3 μm with that for 5 μm silica particles demonstrates the effect of different densities of the particles focused due to the action of the gravitation and buoyancy and the counteracting lift force. The experimental data for 5 μm silica as well as for PSL 5.3 μm particles were obtained at $\Delta T$ = 0 °C. However, the effect of different densities of the retained PSL and silica particles is clearly documented. The dependence $R = f(\langle v(x)\rangle)$ for silica particles lies well below that for PSL particles up to the average linear velocity of the carrier liquid $\langle v_y(x)\rangle$ = 0.417 cm/s. This difference can be explained by much higher density of silica particles ($\rho_{SiO2} \approx 2.1$ g/cm$^3$) which causes their slower takeoff from the lower wall in comparison with PSL particles ($\rho_{PSL} \approx 1.05$ g/cm$^3$). This finding agrees with the theoretical assumptions [15].

Experimental data in Fig. 4 for PSL 1 μm particles, *S. epidermidis* and *R. erythropolis* Gram-positive bacteria were all obtained at the same temperature difference $\Delta T$ = 33 °C and at the temperature of the cold wall, $T_c$ = 21 °C but with the use of carrier liquids containing different concentrations of NaCl: 3 mM/L of NaCl in the case of experiments with PSL 1 μm particles and *R. erythropolis* whereas, and 150 mM/L of NaCl in the case of *S. epidermidis*. The reason for the use of different carrier liquids is explained in the following paragraph in relation with the results shown in Fig. 5. As can be seen in Fig. 4, there are enormous differences in $R = f(\langle v(x)\rangle)$ dependences for the three studied species (PSL, *S. epidermidis*, *R. erythropolis*). These differences cannot be explained by different densities of the retained species (1.03 g/cm$^3$ for PSL, 1.125–1.129 g/cm$^3$ for *S. epidermidis*, as determined in [14], and 1.04 g/cm$^3$ determined by isopycnic focusing in density gradient for *R. erythropolis*) which are very small (in comparison with the effect of density demonstrated by PSL 5.3 μm and silica 5 μm particles). As concerns the size of the retained species, only *R. erythropolis* cells are significantly larger, see the results of the dynamic light scattering (DLS) given in the following paragraphs, but PSL 1 μm and *S. epidermidis* have almost the same size. Substantially higher retention ratios of bacteria cells, within the whole range of average linear velocities of carrier liquid, in comparison with perfectly spherical PSL particles could be due to their non-spherical shape which is more important for *R. erythropolis* than for *S. epidermidis*. This hypothesis is developed below.

Fig. 5 represents the fractograms of *S. epidermidis* obtained at average linear velocity of the carrier liquid $\langle v(x)\rangle$ = 0.208 cm/s but at different temperature differences, $\Delta T$ = 0 °C and $\Delta T$ = 33 °C, and at different concentrations of NaCl in carrier liquid: 3 mM/L and 50 mM/L. As a matter of fact, the first peaks in all fractograms shown in Fig. 5 but also in Figs. 8, 10 and 12, always correspond either to the small-size of unfocused and thus unretained species (for example to the products of bacteria metabolism) or to the large-size species either unfocused or focused near the centerline of the channel (it means at the fastest streamline), or to a mixture of both. Large-size unfocused or focused species can thus move along the channel with an average linear velocity higher than the average linear velocity of the carrier liquid. Such a behavior was confirmed by the fact that some peaks of large-size unfocused or focused species eluted in shorter time in comparison with retention time of the unretained acetone. As can be seen in Fig. 5, the *S. epidermidis* is not retained or is focused near the centerline at $\Delta T$ = 0 °C in carrier liquid containing 3 mM/L of NaCl but it exhibits a small increase in retention with an increase in concentration of NaCl. The increase in concentration of NaCl causes the screening of surface charges, a decrease of zeta-potential (as can be seen in Fig. 6), and thus the reduction of inter-particle repulsive interactions. As a result, the sole gravitational force is able to generate a weak retention indicated by the shoulders on the fractograms. On the other hand, the application of temperature difference $\Delta T$ = 33 °C causes a substantial increase in retention of *S. epidermidis*. It means that *S. epidermidis* exhibits an important thermal diffusion effect. The retention of *S. epidermidis* at $\Delta T$ = 33 °C is also weakly influenced by the variation of the concentration of NaCl in carrier liquid, as can be seen in Fig. 7. Although the decrease of zeta-potential of *S. epidermidis* with increasing concentration of NaCl is important (see Fig. 6), the corresponding variation of retention ratio is almost negligible (see Fig. 7). These findings indicate that there is not an important aggregation of the cells in 150 mM/L NaCl but perhaps the variation of NaCl concentration causes some minor changes in size of *S. epidermidis* which, however, were not confirmed (within the range of experimental errors) by DLS measurements. Particle diameter $d_p$ of *S. epidermidis* was found $d_p$ = 0.89 μm in pure water and $d_p$ = 0.91 μm in 145 mM/L NaCl.

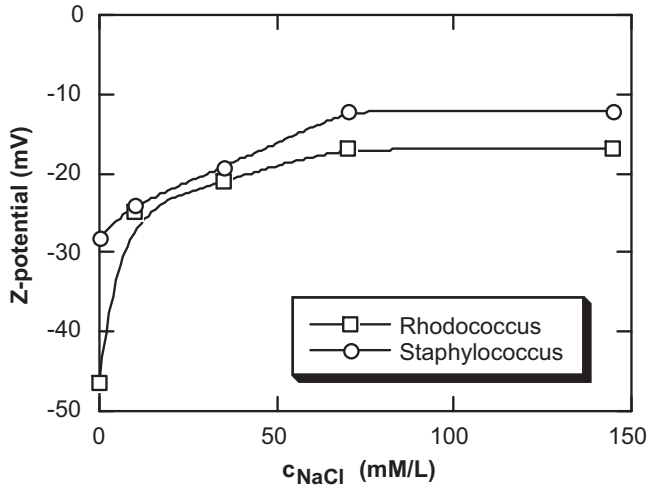


**Fig. 6.** Dependence of the ζ-potential of *Staphylococcus epidermidis* and *Rhodococcus erythropolis* bacteria on the concentration of NaCl in carrier liquid.

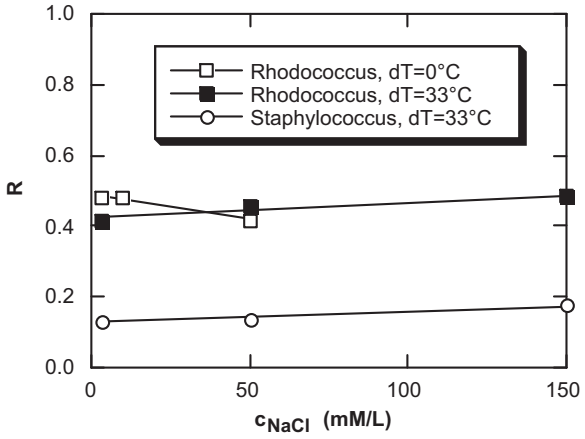


**Fig. 7.** Dependence of the retention ratio $R$ of *Staphylococcus epidermidis* and *Rhodococcus erythropolis* bacteria on the concentration of NaCl in carrier liquid obtained under different experimental conditions of Microthermal Field-Flow Fractionation. Experimental conditions: temperature of the cold wall $T_c = 21\,^{\circ}C$, linear velocity of the carrier liquid during the elution $\langle v(x)\rangle = 0.208$ cm/s, temperature difference, $\Delta T = dT$ is given for each particular experiment.

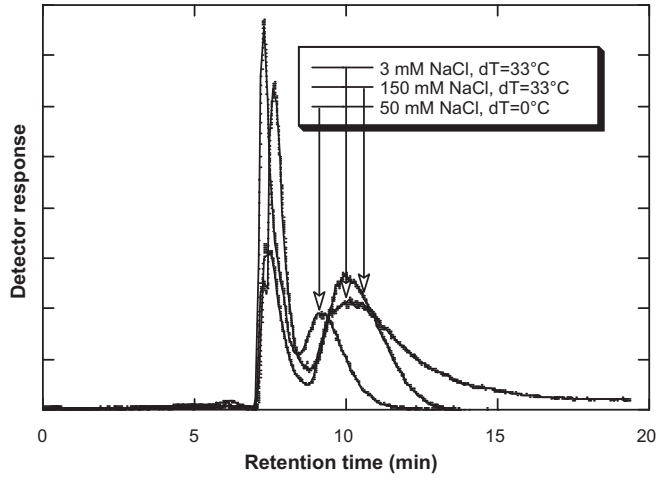


**Fig. 8.** Fractograms of *Rhodococcus erythropolis* cells obtained under different experimental conditions of Microthermal Field-Flow Fractionation. Experimental conditions: temperature of the cold wall $T_c = 21\,^{\circ}C$, linear velocity of the carrier liquid during the elution $\langle v(x)\rangle = 0.208$ cm/s, temperature difference, $\Delta T = dT$ is given for each particular experiment.

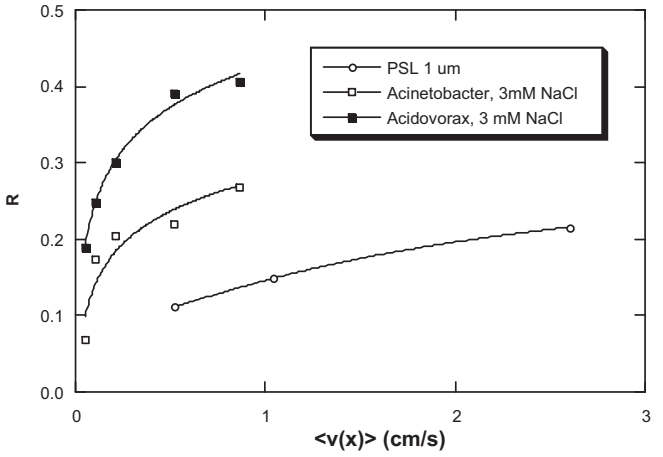


**Fig. 9.** Dependences of the retention ratio $R$ on the average linear velocity of the carrier liquid $\langle v(x)\rangle$ for 1 μm polystyrene latex particles and for *A. lwoffii* and *Acidovorax* sp. bacteria. Experimental conditions: temperature of the cold wall $T_c = 21\,^{\circ}C$, $\Delta T = 33\,^{\circ}C$, linear velocity of the carrier liquid during the elution $\langle v(x)\rangle = 0.208$ cm/s.

Fig. 8 shows the fractograms of *R. erythropolis* obtained at average linear velocity of the carrier liquid $\langle v(x)\rangle = 0.208$ cm/s but at different temperature differences $\Delta T = 0\,^{\circ}C$ and $\Delta T = 33\,^{\circ}C$, and at different concentrations of NaCl in carrier liquid (from 3 mM/L to 150 mM/L). The fractogram obtained at $\Delta T = 0\,^{\circ}C$ indicates that there is a non-negligible retention due to only lift force and the counteracting gravitation-buoyancy force. DLS measurements of *R. erythropolis* indicated a small variation of the size, $d_p = 3$ μm in pure water and $d_p = 2.8$ μm in 145 mM/L NaCl. The application of temperature difference $\Delta T = 33\,^{\circ}C$ leads to an important increase in retention thus showing that this species also exhibits the effect of thermal diffusion. Small and non-systematic variation of retention ratio with the concentration of NaCl in carrier liquid (see Fig. 7) can hardly be related to an important variation of the zeta-potential with the concentration of NaCl (see Fig. 6). However, it is worthwhile to note that a decrease of *R. erythropolis* particle–particle repulsive electrostatic interactions with an increase of NaCl concentration is accompanied by narrowing of the focused zones with increasing concentration of NaCl (see the concerned fractograms in Fig. 8, obtained at $\Delta T = 33\,^{\circ}C$). This observation holds true also for the fractogram obtained at 50 mM/L of NaCl in carrier liquid, not shown in Fig. 8. This is an important finding because it represents the first experimental proof of our theoretical prognosis [15] concerning the narrowing of the focused zones as a consequence of the reduced particle–particle repulsive interactions.

An actual separation of *S. epidermidis* and *R. erythropolis* bacteria was published previously [13]. Fig. 1 in Ref. [13] clearly showed that the order of elution was rod-shaped *R. erythropolis* first, followed by nearly spherical *S. epidermidis*. With regard to relatively high linear velocities of the carrier liquid, $\langle v(x)\rangle = 0.208$ cm/s, focusing mechanism clearly dominated the separation.

### 4.2. Retention of Gram-negative bacteria

The comparison of $R = f(\langle v(x)\rangle)$ dependence for PSL 1 μm particles with those for *A. lwoffii* and *Acidovorax* sp. is shown in Fig. 9. The differences in $R = f(\langle v(x)\rangle)$ dependences for the PSL particles and Gram-negative bacteria are similar to those of Gram-positive bacteria presented in Fig. 4. *A. lwoffii* is known as nonmotile cocci which usually occurs in pairs under magnification. The size of our sample measured by DLS was $d_p = 1.1$ μm in pure water and $d_p = 1.3$ μm in 145 mM/L NaCl, thus very close to the size of PSL particles. The density of *A. lwoffii* determined by isopycnic focusing was $\rho_{Ac} \approx 1.09\ g/cm^3$. *Acidovorax* sp. consists mainly of single

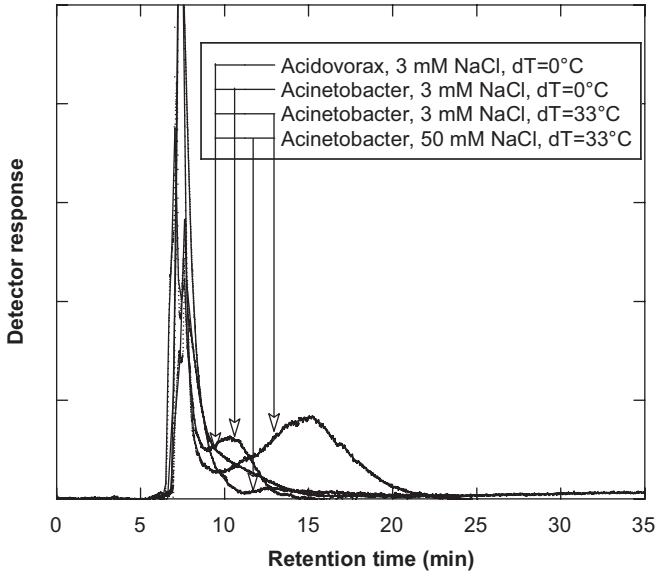


**Fig. 10.** Fractograms of *A. lwoffii* and *Acidovorax* sp. cells obtained under different experimental conditions of Microthermal Field-Flow Fractionation. Experimental conditions: temperature of the cold wall $T_c = 21\,^{\circ}C$, linear velocity of the carrier liquid during the elution $\langle v(x)\rangle = 0.208$ cm/s, temperature difference, $\Delta T = dT$ is given for each particular experiment.

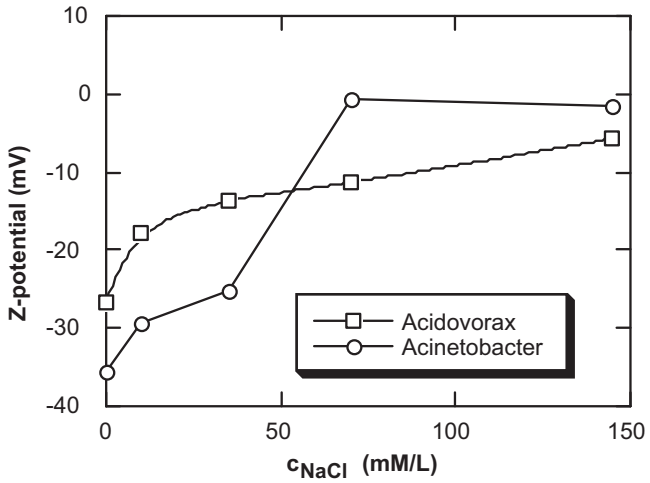


**Fig. 11.** Dependence of the ζ-potential of *A. lwoffii* and *Acidovorax* sp. bacteria on the concentration of NaCl in carrier liquid.

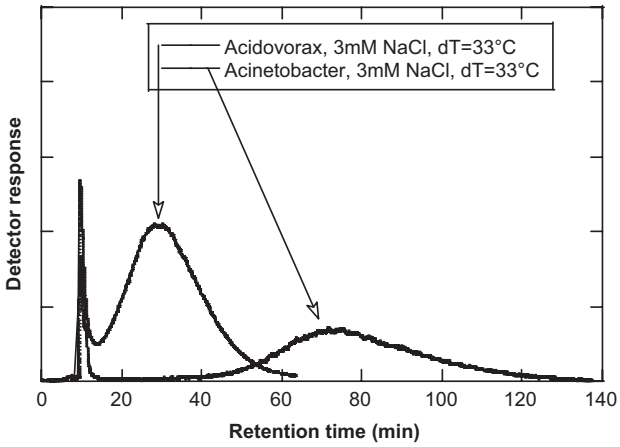


**Fig. 12.** Fig. 5 Fractograms of *A. lwoffii* and *Acidovorax* sp. cells obtained by Microthermal Field-Flow Fractionation under identical experimental conditions. Experimental conditions: temperature of the cold wall $T_c = 21\,^{\circ}C$, temperature difference, $\Delta T = dT = 33\,^{\circ}C$, linear velocity of the carrier liquid during the elution $\langle v(x)\rangle = 0.052$ cm/s.

rod cells with the width of 0.8 μm (ranging from 0.6 to 0.9 μm) and the length of 1.6 μm (ranging from 1.0 to 2.1 μm). The pairs of cells with the length of 2.8 μm (ranging from 2.2 to 3.6 μm) are usually present. The size of our sample of *Acidovorax* sp. determined by DLS was $d_p = 2.1$ μm in 145 mM/L NaCl. The density of *Acidovorax* sp. was not measured but should lie within the range of densities of all other bacteria studied in this work. As a result, also in this case of Gram-negative bacteria, an important difference between $R = f(\langle v(x)\rangle)$ dependences for bacteria cells and that for PSL particles cannot be explained by the differences in size or density.

Fig. 10 represents the fractograms of *A. lwoffii* and *Acidovorax* sp. obtained at average linear velocity of the carrier liquid $\langle v(x)\rangle = 0.208$ cm/s but at different temperature differences, $\Delta T = 0\,^{\circ}C$ and $\Delta T = 33\,^{\circ}C$, and at different concentrations of NaCl in carrier liquid (3 mM/L and 50 mM/L). As can be seen in Fig. 10, *A. lwoffii* exhibits a clear retention in carrier liquid containing 3 mM/L of NaCl, even at $\Delta T = 0\,^{\circ}C$, which is again due to only lift force and counteracting gravitation-buoyancy force. Its retention substantially increases at temperature difference of $\Delta T = 33\,^{\circ}C$ in 3 mM/L NaCl but it decreases in 50 mM/L NaCl. This spectacular decrease in retention coincides with a dramatic decrease of zeta-potential of *A. lwoffii* within the range of concentrations 35 mM/L to 70 mM/L of NaCl, as can be seen in Fig. 11. Such a dramatic decrease of zeta-potential can provoke the aggregation of *A. lwoffii* cells which was not detected by DSL measurement in 145 mM/L NaCl solution because of relatively low concentration of the cells. On the other hand, such an aggregation might occur under Microthermal FFF conditions due to the important concentration of the cells within the focused zone. The formed large aggregates are focused near the centerline of the channel and are then transported by carrier liquid at faster velocity. It results in an increase of retention ratio, as already discussed above.

*Acidovorax* sp. exhibits only a weak retention at $\Delta T = 0\,^{\circ}C$ in carrier liquid containing 3 mM/L of NaCl and at average linear velocity of the carrier liquid $\langle v(x)\rangle = 0.208$ cm/s (see the shoulder on the corresponding fractogram in Fig. 10). On the other hand, a decrease of average linear velocity of the carrier liquid to $\langle v(x)\rangle = 0.052$ cm/s and the application of temperature difference of $\Delta T = 33\,^{\circ}C$ in 3 mM/L NaCl resulted in an important increase of the retention of *Acidovorax* sp., as can be seen in Fig. 12. The fractogram of *A. lwoffii*, shown in Fig. 12, was obtained under the identical experimental conditions and demonstrates that the difference in the retentions of these two Gram-negative bacteria should allow their separation. In this case of Gram-negative bacteria, the elution order was the same as in the case of Gram-positive bacteria. The rod-shaped *Acidovorax* sp. eluted first, followed by nearly spherical cells of *A. lwoffii*. On the other hand, with regard to lower linear velocity of the carrier liquid applied in this case, $\langle v(x)\rangle = 0.052$ cm/s, polarization mechanism probably dominated the separation.

## 5. Conclusions

The theoretical analysis concerning free translational and rotational diffusion of the spherical and non-spherical particles, exposed to temperature gradient and, consequently, undergoing the thermophoresis, indicated the possibilities to fractionate the particles according to the differences in shape.

Orientation of the spherical and non-spherical particles caused by topographical heterogeneity of their surface chemical nature or by heterogeneous dissipation of heat energy due to non-homogeneous thermal conductivity of the particle body can also be

exploited for the fractionations based on the differences in shape of the cells and subcellular particles.

An optimized choice of the operational conditions, especially of temperature gradient and linear velocity of the longitudinal flow of carrier liquid should allow the above mentioned separations of the particles by Microthermal Field-Flow Fractionation. Both main separation mechanisms, polarization and focusing, seem to be effectively exploited.

Preliminary experimental separations of nearly spherical and rod-shaped Gram-positive and Gram-negative bacteria confirmed that Microthermal Field-Flow Fractionation is a suitable method to perform such difficult task. Although the preliminary experimental results are convincing, it is obvious that enormous but challenging experimental work remains to be done in order to fully exploit the potential of Microthermal Field-Flow Fractionation in cells and subcellular particles separations.

In the theoretical part, all possible explanations of the experimental results were analyzed and discussed. The analysis showed that the only explanation of the separation of different bacteria is based on the differences in their shape. The goal of our study was to compare qualitatively the experimental observations with the contributions of some particular mechanisms participating in the separations of the spherical and non-spherical particles and described in the theoretical part. The investigated system is so complex that quantitative comparison is recently not possible with regard to the lack of full understanding of thermal diffusion phenomenon.

## Acknowledgements

This work was partially supported by the Ministry of Education, Youth and Sports of the Czech Republic, project No. MSM 7088352101. Dr. V. Kašpárkova provided the DLS and ζ-potential data, Dr. A.Yu. Menshikova provided PSL particles, and Dr. M. Minárik provided silica particles.

## References

[1] D.S. Kompala, P. Todd (Eds.), Cell Separation Science and Technology, ACS Symposium Series 464, American Chemical Society, Washington, DC, 1991.
[2] J. Janča, M. Špírková, J. Stejskal, Russian J. Phys. Chem. 77 (Suppl. 1) (2003) S95.
[3] J. Janča, Phys. Chem. Chem. Phys. 2 (2000) 2607.
[4] J. Janča, N. Gospodinova, Sep. Purif. Methods 29 (2000) 247.
[5] D.W. Qi, Int. J. Mod. Phys. C 80 (1997) 98.
[6] D.W. Qi, J. Fluid. Mech. 385 (1999) 41.
[7] X. Rong, D. Qi, G. He, J.Y. Zhu, T. Scott, Comp. Math. Appl. 55 (2008) 1560.
[8] J.Z. Lin, X. Shi, Z.J. You, Aerosol. Sci. 23 (2003) 909.
[9] B. Herzhaft, E. Guazzelli, M.B. Mackaplow, E.S.G. Shaqfeh, Phys. Rev. Lett. 77 (2) (1996) 290.
[10] M.B. Mackaplow, E.S.G. Shaqfeh, J. Fluid. Mech. 376 (1998) 149.
[11] B. Herzhaft, E. Guazzelli, J. Fluid. Mech. 384 (1999) 133.
[12] J.C. Bigelow, Y. Nabeshima, K. Kataoka, J.C. Giddings, in: D.S. Kompala, P. Todd (Eds.), Cell Separation Science and Technology, ACS Symposium Series 464, American Chemical Society, Washington, DC, 1991, p. 146.
[13] V. Kašpárková, V. Halabalová, L. Šimek, J. Růžička, J. Janča, J. Biochem. Biophys. Methods 70 (2007) 685.
[14] J. Janča, V. Kašpárková, V. Halabalová, L. Šimek, J. Růžička, E. Barošová, J. Chromatogr. B 852 (2007) 512.
[15] J. Janča, Microthermal Field-Flow Fractionation: Analysis of Synthetic, Natural, and Biological Macromolecules and Particles, HNB Publishing, New York, 2008.
[16] J. Janča, I.A. Ananieva, A.Yu. Menshikova, T.G. Evseeva, J. Chromatogr. B 800 (2004) 33.
[17] J. Janča, J. Stejskal, I.A. Ananieva, J.-F. Berneron, J. Gearing, M. Minárik, in: M.M. Bou-Ali, J.K. Platten (Eds.), Thermodiffusion: Basics & Applications, Mondragon Unibersitatea Press, 2006, p. 337.
[18] G. Stokes, Mathematical and Physical Papers, Cambridge Univ. Press, New York, 1880.
[19] A. Einstein, Ann. Phys. &LPKT;Berlin&RPKT; 19 (1906) 371.
[20] H. Morawetz, Macromolecules in Solution, John Wiley & Sons, New York:, 1965.
[21] F. Perrin, J. Phys. Radium 7 (1936) 1.
[22] J. Riseman, J.G. Kirkwood, J. Phys. Chem. 18 (1950) 512.
[23] R. Gans, Ann. Physik &LPAR;4&RPAR; 86 (1928) 628.
[24] F. Perrin, J. Phys. Radium 5 (1934) 497.
[25] J. Janča, J. Stejskal, J. Chromatogr. A 1216 (2009) 9071.
[26] L.D. Landau, E.M. Lifschitz, Statistical Physics, 3rd edition, Butterworth-Elsevier, New York, 1980.
[27] D. Kondepudi, I. Prigogine, Modern Thermodynamics: From Heat Engines to Dissipative Structures, John Wiley & Sons, Chichester, 1998.
[28] K.D. Caldwell, T.T. Nguyen, M.N. Myers, J.C. Giddings, Sep. Sci. Technol. 14 (1979) 935.